IEEE Access
Multidisciplinary | Rapid Review | Open Access Journal

Received December 1, 2020, accepted December 18, 2020, date of publication December 22, 2020, date of current version January 6, 2021.

Digital Object Identifier 10.1109/ACCESS.2020.3046651

Method for Vortex Shape Retrieval and Area Calculation Based on Convex Hull Algorithm

XU WEI[1,2], JIYU LI[1,2], BO LONG[1,2], XIAODAN HU[1,2], HAN WU[1,2], AND HUIFEN LI[3]

[1]College of Engineering, South China Agricultural University, Guangzhou 510642, China
[2]National Center for International Collaboration Research on Precision Agricultural Aviation Pesticides Spraying Technology, Guangzhou 510642, China
[3]Rice Research Institute, Guangdong Academy of Agricultural Science, Guangzhou 510640, China

Corresponding author: Jiyu Li (lijiyuscau@qq.com)

This work was supported in part by the National Natural Science Foundation of China under Grant 31771682, and in part by the Science and Technology Planning Project of Guangdong Province under Grant 2018A050506073.

ABSTRACT The shape and area of the vortex are important indicators to judge the effect of chemical liquid spraying and crop pollination by agricultural plant protection UAV. However, the traditional way of extracting the vortex related data through manual methods without an adaptive mechanism is complicated and inefficient. In order to solve this problem, the vortex image is preprocessed by adaptive iterative binarization and mean filtering. Then, the Convex Hull algorithm combined with Edge function is applied to the pre-processed image to extract the specific shape of vortex image and further calculate its area. Experimental results show that this method can be used to extract the vortex shapes and calculate the vortex area under different experimental conditions without manual intervention. Compared with the results of vortex area obtained via the manual extraction method, this method reported the average absolute error rate of 2.84%, the RMSE of 0.2903, and the correlation coefficient of 0.9965, indicating that the proposed method is more applicable to reveal the actual state of the vortex. A standardized extraction method was established to provide a standard for future vortex image research. The method in this paper lays a scientific foundation for the real-time tracking research of agricultural plant protection UAV and vortex.

INDEX TERMS Agricultural plant protection UAV, convex hull algorithm, edge retrieval, shape and area, vortex.

I. INTRODUCTION

As agricultural plant protection UAVs are widely used in precision agriculture, the UAVs are required to fulfil more precise and efficient operation tasks in actual agricultural plant protection practices. To this end, in-depth analysis and research on the operation process of the UAV are of more necessity and importance. The phenomenon that the crop canopy significantly changes shape under the interaction between itself and the downward rotor airflow generated by the UAV is generally called vortex in this paper. In the process of spraying pesticide, the rotor airflow generated by the UAV wraps the pesticide droplets and penetrates the crop from top to bottom, which is conducive to the uniform distribution of the droplets on various parts of the plant [1]. Therefore, it is one of the effective methods to improve the deposition and uniform distribution of effective pesticides on the crops. During the operation of the UAV, the distribution of droplets is not only related to the operation parameters of the UAV itself, but also has a significant correlation with the wind field, including rotor airflow wind field and surroundings wind field [2]. Therefore, during the UAV spraying operation, the vortex shape and area data at the crop canopy level are important indicators to measure the pesticide spraying effect. Similarly, utilizing the rotor airflow wind field generated by the UAV can help facilitate pollination operations [3]. In summary, the shape and area data of the vortex during the UAV operations are important descriptors of the chemical liquid spraying and crop pollination. It is the foundation for the real-time follow-up study of the vortex and the UAV. However, very few researches are available on the shape retrieval and area calculation of the vortex, due to the three unique and complex features:

1) High integration of foreground and background. During the operation of agricultural plant protection UAVs, influenced by the airflow of the rotor, a follower vortex as the foreground is formed at the crop canopy, while the rest of the crops serve as the background, both

The associate editor coordinating the review of this manuscript and approving it for publication was Geng-Ming Jiang.

of which are hard to segment because they are highly integrated with each other.

2) Noise interference. A lot of isolated noise points on the edge of the vortex, together with the external factors like device properties and transmission media, pose substantial random interference on the image and make it hard to guarantee the image quality during the image acquisition process.
3) Sawtooth edge. The edge of the vortex is composed of the fallen and unfallen crops under the rotor airflow. Vortex edge changes are not obvious or regular. There are areas with gentle transitions at the edges, exhibiting a nonlinear continuous sawtooth state.

Scholars at home and abroad have conducted a lot of researches concerning the above three image features by means of various methods. Although no research has been conducted on separating the foreground and the background with highly integrated features of the vortex image so far, insights for this regard can be drawn from the following studies. Xue Ping proposed an image foreground and background segmentation algorithm that used a classifier to extract color and texture from the image super-pixel to separate the foreground and background [4]. Liao Juan *et al.* presented a nonparametric approach to foreground detection in dynamic backgrounds [5]. Yurong Li published a Fractal Dimension-based approach to index, segment or classify texture images [6]. Yang Yi advocated a method of image quantification based on local texture features [7]. Hosang Jan *et al.* suggested an object selection algorithm using binarized normed gradient to screen candidate areas based on the edge detector [8]. The above-mentioned studies are based on the color, brightness, and texture of the foreground to preprocess the grayscale image, after which the foreground image is extracted through algorithms. Although the application of image preprocessing methods such as mean filtering and binarization to the vortex image can protrude the vortex body and reduce interferences like noises, it can't produce the vortex edge image since the foreground (vortex) and the background (crops) are not clearly separated. This is because the vortex and the crop are not independent units but integrated parts of the crops with no obvious differences in color and texture.

There are some thought-provoking studies for the discussion of the nonlinear continuous sawtooth edge feature of the vortex image. The research team headed by Dong Yahan applied the convex hull algorithm based on the tree crown outline points, and accurately obtained the canopy surface information [9]. To extract egg contours, Duan Yufei and others adopted the morphological fitting in combination with the convex hull algorithm [10]. Cupec Robert *et al.* employed the convex hull algorithm for targeted object recognition [11]. Xiao Lin *et al.* utilized a convex hull prior to detect salient objects [12]. By applying the above method to the vortex research, it is found that although the convex hull algorithm can identify the position and scope of the vortex body, it cannot clearly show the sawtooth edge feature. Moreover, the convex hull algorithm produces only convex images of vortex edge contour, among which there are some weak edges and false edges [13]. The key to vortex related information extraction lies in the accurate edge retrieval in light of the three vortex features.

Based on the above research contents, the purpose of this study is to propose a method that can highlight the vortex body, reduce noise interference, effectively deal with the sawtooth edge presented in the vortex [14], draw a vortex edge closure image, and extract the shape of the vortex body and calculate its area in an adaptive way without manual intervention.

The contributions of this paper are summarized as follows:

- We propose a method for drawing the shape of vortex and calculating its area based on convex hull algorithm. This method can combine convex hull algorithm and edge function skillfully by means of self-adaptive binarization iteration method and filtering method, and then extract eddy vortex image and calculate its area effectively.
- A vortex image acquisition system is designed to validate the proposed method. It is proved that our method can be applied to different experimental environments, can be adaptive to extract the vortex image without manual intervention, and the extracted vortex image has a good effect.
- A standardized extraction method was established to provide a standard for future vortex image research. It lays a foundation for the follow-up study of agricultural plant protection UAV and vortex.
- To provide the corresponding data in the field operation for measuring the spraying effect of aviation operation.

The reminder of this article is organized as follows. The proposed method is introduced in Section II, and the experimental results and analysis are shown in Section III. We conclude the article in Section IV.

II. ARCHITECTURE

In this section, we focus on the analysis of the three features of the vortex image, and proposes a method for vortex shape retrieval and area extraction based on the convex hull algorithm. This method is composed of five parts: 1) the vortex image acquisition system; 2) the image preprocessing; 3) the vortex edge retrieval; 4) the vortex shape drawing; and 5) the vortex area calculation. Image preprocessing can be further divided into three modules: Graying, Mean filtering and Binarization. The vortex edge retrieval is the core of this method. The overall technical flow of our proposed method is shown in Fig.1.

A. VORTEX IMAGE PREPROCESSING

At present, it is difficult to accurately retrieve the vortex shape and extract its area without an accurate adaptive vortex edge retrieval method that concerns the three characteristics of the vortex image. To fill this gap, the first task is to accurately retrieve the vortex edge. Considering the three features of the

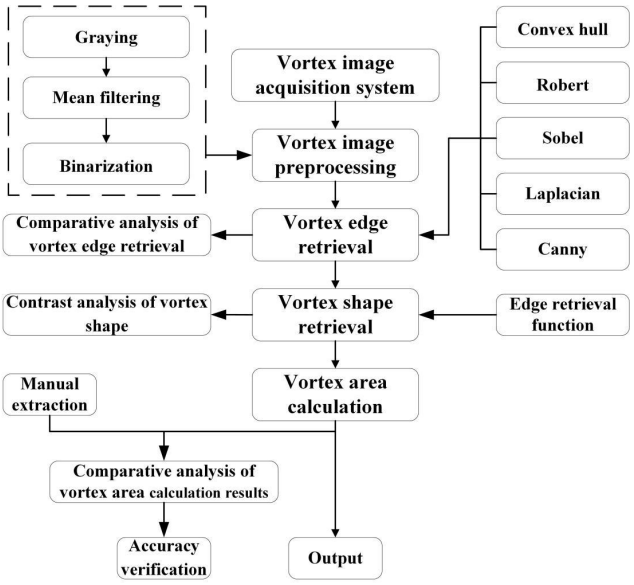

FIGURE 1. Flow chart of the proposed method.

vortex image, it is necessary, for the sake of accurate and effective edge retrieval, to preprocess the image to reduce noise interference and raise image contrast. The vortex image was first converted into a gray image to raise its contrast, and then undergone mean filtering to smooth the image for the purpose of reducing noise interference. Finally, binarization was utilized to protrude the vortex body.

In the existing studies, PSNR was used to select the appropriate mean filter kernel [15]. The larger the PSNR value, the smaller the image distortion, as shown in Equation 1-2.

$$PSNR = 10 \times lg\left(\frac{Max_I^2}{MSE}\right) \tag{1}$$

$$MSE = \frac{1}{mn}\sum_{i=0}^{m-1}\sum_{j=0}^{n-1}\|I\,(i,j) - K(i,j)\|^2 \tag{2}$$

Max_I represents the maximum value of the image color. MSE is the mean square error between the original image and the processed image. $I\,(i,j)$, $K(i,j)$ stands for original and processed image.

In order to obtain the optimal binarization threshold that can be adaptive generated according to different vortex images, the iterative method based on the approximation idea was adopted to obtain it [16]. The steps are as follows:

1). Figure out the maximum and minimum grayscale values of the image, mark them as Z_{max} and Z_{min}, and set the initial threshold value as T_0, as shown in Equation 3).

$$T_0 = \frac{Z_{max} + Z_{min}}{2} \tag{3}$$

2). According to the threshold value $T_k = T_0$, the gray value of the image was divided into two parts, and the average gray value Z_a and Z_b are obtained, respectively.

3). Find the new threshold T_{k+1}, as shown in Equation 4.

$$T_{k+1} = \frac{Z_a + Z_b}{2} \tag{4}$$

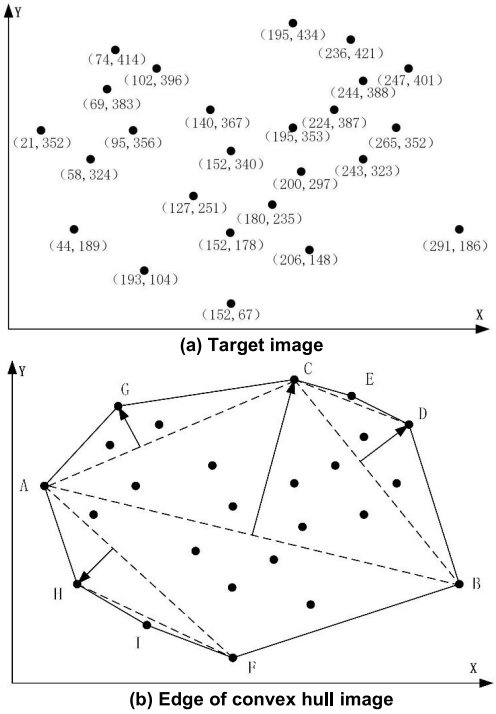

FIGURE 2. Convex hull algorithm and application.

4). If $T_k = T_{k+1}$, the obtained value is the optimal threshold. Otherwise, go back to the step 2 and continue the iterative calculation until the optimal threshold is found.

B. VORTEX EDGE RETRIEVAL

In existing research, consider three features of the vortex image, the convex hull algorithm is advisable for edge contour retrieval. Convex hull algorithm, a computational geometry method, effective in irregular edge retrieval, is often used to identify the shape or contour of an object [17]. With reference to the isolated edge noise points and the sawtooth feature of the vortex edge image, cycle recursion was adopted to sort and scan the points inside the convex hull. The furthest point named as pole was retrieved from the convex hull image point set and connected to form the dividing line of convex hull. Then the furthest point from the dividing line was scanned as the new pole and connected. Recursive algorithm was repeated to calculate the convex hull until the algorithm can't come up with any new poles.

The convex hull algorithm was used to briefly extract isolated points from the vortex image. A coordinate system was constructed with the lower left corner as the origin, in which every isolated point on the image is positioned, as shown in Fig.2a. Two polar points marking (21, 353) and (291, 186) were labelled Point A and Point B, respectively. The line connecting Point A and Point B divided the whole image into two convex hulls, the upper and the lower. Recursive algorithm was employed to find Point C (195, 434) which was the farthest from Line AB. Point C was connected to Point A and Point B to form Line AC and Line BC. Recursive algorithm was repeated to calculate the convex hull with A

and C, B and C as two groups of polar points. Such operation was repeated until the convex hull corresponding to the two polar points couldn't be found. Under such circumstance, the farthest point is the convex hull vertex. The convex polygon AECFDBGIH (Fig.2b) of the vortex edge image is finally obtained through the recursive cycle.

C. VORTEX SHAPE RETRIEVAL

After obtaining the small convex hull of the vortex body edge and other parts of the image, in order to further define the vortex shape, the Find-Contours function and the Draw-Contours function were used to process the vortex convex hull image and outline the vortex edge. All the edges of the closed contours were retrieved from the convex hull image of the vortex. Based on the pixel statistics in the closed contour, vortex shape image was obtained after eliminating minor closed contours by filtering. Based on the pixel statistics in the closed contour, the largest contour image in the image is the vortex shape. After eliminating minor closed contours by filtering, the vortex shape image was obtained.

D. VORTEX AREA CALCULATION

The area (i.e. pixels in the closed contour) of the vortex and reference plate was counted. At the same time, the actual area of the horizontal reference plate was 0.324m^2 (the actual size: 60cm×54cm). From the Equation 5, the actual area of the vortex was measured [18].

$$\frac{S}{s} = \frac{M}{m} \tag{5}$$

S represents the vortex area; s refers to the reference plate area; M stands for the vortex area pixels; m is for the reference plate area pixels.

E. ACCURACY VERIFICATION

Since the actual area of the vortex cannot be directly obtained and set up sensors in the field will affect the formation of the vortex, manual method is often used to draw the vortex contour and calculate the actual vortex area as the reference value for further measurement and comparison. The vortex area result obtained via manual extraction, though not of absolute accuracy, produced accurate and reliable vortex contour by analyzing the progressively changing vortex image.

The absolute error rate (p, Equation 6), RMSE (root mean square error, Equation 7) and correlation coefficient (r, Equation 8) were used to compare with the results obtained via the manual extraction method, the method proposed in this paper. Based on the analysis of these parameters, it is used to verify the accuracy of vortex shape extraction and area calculation.

$$\text{p} = \left| \frac{\text{A}_\text{i} - \text{B}_\text{i}}{\text{A}_\text{i}} \right| \times 100\% \tag{6}$$

$$\text{RMSE} = \sqrt{\frac{1}{\text{m}} \sum_{\text{i}=1}^{\text{m}} (\text{A}_\text{i} - \text{B}_\text{i})^2} \tag{7}$$

$$\text{r}_{\text{AB}} = \frac{\sum_{\text{i}=1}^{\text{m}} (\text{A}_\text{i} - \bar{\text{A}})(\text{B}_\text{i} - \bar{\text{B}})}{\sqrt{\sum_{\text{i}=1}^{\text{m}} (\text{A}_\text{i} - \bar{\text{A}})^2} \sqrt{\sum_{\text{i}=1}^{\text{m}} (\text{B}_\text{i} - \bar{\text{B}})^2}} \tag{8}$$

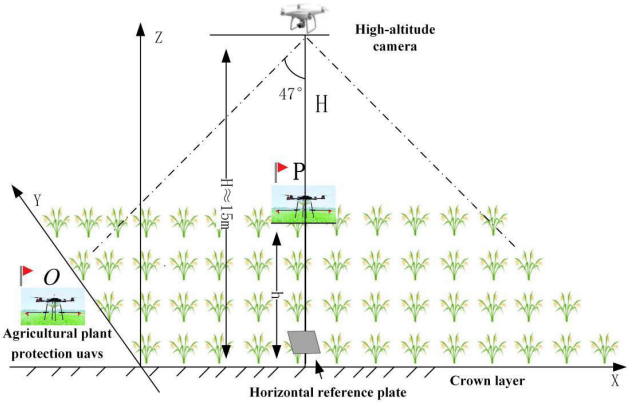

FIGURE 3. Vortex image acquisition system.

m is the total number of samples, A_i represents the reference value and B_i refers to the reference value. $\bar{\text{A}}$, $\bar{\text{B}}$ is the sample mean value.

III. EXPERIMENTS AND ANALYSIS

A. ACQUISITION OF VORTEX IMAGES

The image data acquisition was carried out at Baiyun Test Base (23°23′47.98"N, 113°26′11.79"E) of Guangdong Academy of Agricultural Sciences. The vortex image acquisition system, as Fig.3 shows, is composed of high-altitude camera and agricultural plant protection UAV. DJI "Phantom 4" UAV (Shenzhen, China) served as the high-altitude camera in this test to take RGB images of the vortex, and the lens parameters are 4096∗2160(p∗p) FOV 94°20 mm, as Fig.2c shows. The horizontal reference plate was placed flush with the rice crown. The specific experimental process was as follows: Firstly, the high-altitude camera UAV takes off and then hovers at a height of 15m above the rice canopy to start shooting video. It is necessary to ensure that the preset horizontal reference plate is directly below the camera. Secondly, the agricultural UAV takes off from Starting Point O, and hovers directly below the UAV at Point P to form a stable vortex. The agricultural UAV create dynamic vortex images by hovering or flying horizontally. After completing the scheduled experimental flight mission, and then the UAV flies back to the Starting Point O. The camera UAV returns and sends the vortex video to the computer for image preprocessing.

In order to ensure the universality of the method described in this paper, vortex images under different growth stages and field densities of rice, flight status, light conditions, rotor number of the UAV, and wind force conditions were collected as verification tests, as Fig.4a-f and Tab.1 shows. These tests are conducted as the schematic diagram of the vortex image acquisition system shown in Fig.3. In particular, the UAV of the Test 2 was spraying chemicals.

Take Test 1 as the main research object, as Fig.4d shows.

B. COMPARATIVE ANALYSIS OF THE VORTEX EDGE RETRIEVAL

Traditional edge detection algorithms using image edge mutation properties to detect edges can be categorized into

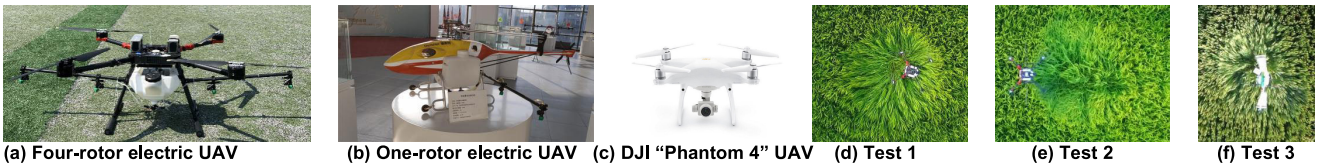

FIGURE 4. Experimental equipment and vortex images.

TABLE 1. Field property information for each test

Group	Time	Growth Stage	Plant Height (mm)	Plant Density (plant/m^2)	Light conditions	Wind speed[1] (m/s)	Rotor number	Flight status
Test 1	October 21, 2019	Mature Stage	118-120	135	Cloudy	0.8	4	Hover
Test 2	October 20, 2019	Mature Stage	110-115	131	Sunny	0.2	4	Horizontal
Test 3	June 14, 2019	Tillering Stage	85-105	113	Sunny	0.3	1	Hover

[1]Data was collected by Kestrel 5500 Link Micro-weather station (State of California, American)

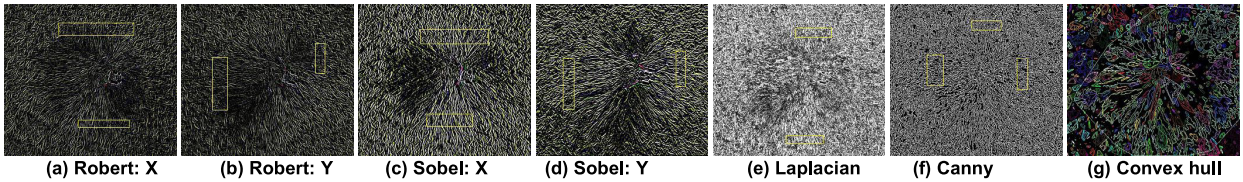

FIGURE 5. Edge algorithm comparison.

two types [19]: one is to detect image edges by calculating the gradient value of the image on the basis of the first derivative edge detection algorithms (e.g. Roberts algorithm and Sobel algorithm); another is to detect through zero-crossing in light of the second derivative (e.g. Laplacian algorithm and Canny algorithm).

In-depth comparative analysis is conducted on the results of vortex edge retrieval using traditional algorithms and convex hull algorithm, as it is shown in Fig.5.

The conventional clear edge can be clearly identified by using Roberts algorithm and Sobel algorithm to retrieve the vortex edge [20], indicating that these two algorithms are applicable in cases where the edges are clear. However, when the edge of the vortex image is unclear, discontinuous and full of noise, Roberts algorithm was found invalid (see yellow boxes in Fig.5a-b). Although the Sobel algorithm has good retrieval accuracy to a certain extent on the gray value gradient and more noisy images. Similarly, it is not possible to detect valid edges in the vortex image (as shown in the yellow boxes of Fig.5c-d).

On the other hand, Laplacian algorithm [21] and Canny algorithm [22] based on the second derivative outperformed Roberts algorithm and Sobel algorithm in reducing noise interference. But on the other hand, as Fig.5e illustrates, the use of higher-order differentials on the edge processing of the image actually makes the vortex edges more blurred, far from satisfactory. Although Canny algorithm can present the sawtooth edges of the vortex, it cannot effectively segment the edges of the vortex image due to the excessive details on the edge (Fig.5f). Moreover, weak edges and pseudo-edges (see yellow boxes in Fig.5f) were identified during the retrieval process, forming many discontinuous edges, which is not conducive to the formation of closed contour edges[23]. In sharp contrast to other methods, the convex hull algorithm applied in this paper takes into consideration the three features of the vortex image for edge retrieval, as shown in Fig.5g. After effective combination of image preprocessing, based on the marginal depression formed by connecting the isolated points at the tip, the convex hull algorithm is capable of obtaining the convex hull image of the vortex and detecting the contour edge of the vortex body and the effect is remarkable.

C. CONTRAST ANALYSIS OF VORTEX SHAPE

The shape of vortex is closely related to the selection of binarization threshold and average filter kernel. In order to obtain accurate vortex images and facilitate the later extraction of corresponding image regions, in-depth research and discussion are carried out.

1) SELECTION OF BINARIZATION THRESHOLD

Binary image processing is an important image processing method, which can effectively segment the background and target image. Image binarization methods are mainly divided into global threshold method and local adaptive

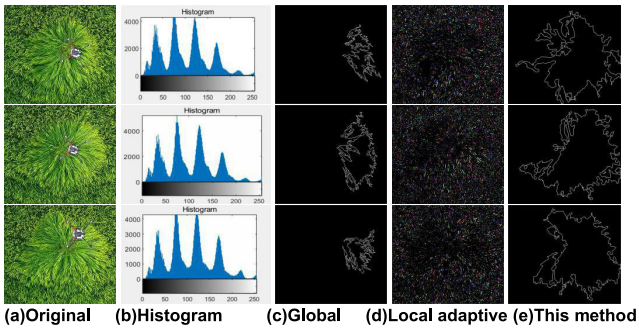

FIGURE 6. Comparison results of binarization methods.

threshold method. The global threshold refers to the selection of a fixed threshold for image binarization based on the whole image, while the local adaptive threshold determines the binarization threshold based on the pixel value distribution of the pixel neighborhood block. The binarization threshold of each pixel in the local adaptive threshold method is not completely consistent. The method is suitable for an image containing noise and non-uniform illumination, and so on and so forth. These two methods were compared with the adaptive binarization threshold iterative method adopted in this paper, as shown in Fig.6.

Three vortex images with different shapes were extracted from Test 1, as shown in Fig.6a. The gray histogram of the vortex image was shown in Fig.6b. It can be seen from the figure that the vortex image is different from the conventional image, and its gray histogram shows multiple peaks, and the distribution of images of different shapes is similar. If the global threshold method was adopted for processing, the commonly adopted threshold value was gray value 128, as shown in Fig.6c. Although different thresholds can be set according to different vortex images to obtain their exact edges, this method cannot form a unified standard and cannot be adaptive to obtain the shapes of different vortex images. If the local threshold method was adopted, the result was shown in Fig.6d. Effective vortex edge image cannot be drawn, and thus vortex shape image cannot be further drawn, indicating that this method was not applicable either. According to the gray histogram of the vortex images, the difference lies in that different gray values correspond to different number of pixel values. The characteristics of different gray values corresponding to different number of pixels were taken into account when processing different vortex images, and the uneven distribution of light in the image was also considered. The method of adaptive binarization iteration threshold was adopted. According to this method, the corresponding binarization threshold for different vortex images can be obtained adaptively without manual intervention, and the difference caused by the influence of light in images can also be eliminated. After applying the iterative binarization threshold optimization operation in this method, the thresholds of the three images were 102, 103 and 106, respectively. The vortex shape images obtained by using this method was shown in Fig.6e.

TABLE 2. PSNR of different kernels

Kernel	3×3	5×5	7×7	9×9	11×11	13×13
PSNR	17.1164	18.6801	19.5264	20.0987	20.5214	20.8559

2) FILTER KERNEL SELECTION

The results of PSNR and the appropriate threshold were compared on the vortex image [24]. As shown in Tab.2, with the increase of the mean filter kernel, the PSNR value increases gradually. As the filtering kernel increases, the pseudo-edge of the vortex edge image decreases gradually, as shown in the yellow border in Fig.7a∼c. However, if the filtering kernel continues to increase, its edge image will sag inward, resulting in the missing of the vortex edge[25]. The results of the vortex shape image overlaid on the original were shown in Fig.7e-f. It can be concluded that the change of filter kernel only affects the extraction of details of vortex edge.

As shown in the Fig.7, the mean filtering with a kernel of 9×9 performed better in defining the vortex shape by removing pseudo-edges and weak edges. Under visual inspection, this indicates that the proposed method can detect the true edge of the image and draw an accurate vortex shape image.

To sum up, the method in this paper processes the image according to the three characteristics of vortex. For the vortex image has a lot of noise points and the edge is fuzzy, the image preprocessing method is adopted, which is mainly adaptive binarization method and mean filtering. Then, the convex hull algorithm is applied to the pre-processed vortex image to obtain the range of the vortex body. In this paper, other existing edge retrieval methods cannot draw the edge of objects with sawtooth edges such as vortex, which proves the superiority of convex hull algorithm. The edge Find-Counters and Draw-counters function are further used to draw and extract the edge of the vortex image. After filtering out the redundant edge, the exact shape of the scroll image is finally obtained. A unified standard was established for the future extraction of vortex images.

D. VERIFY THE UNIVERSALITY OF THE PROPOSED METHOD

The method in this paper was applied to Test 2 and 3, as shown in Fig.9.

According to the method in this paper, it is proved that under different experimental conditions, the accurate vortex shape image can be obtained with the adaptive change of binarization threshold (120 in Test 2 and 116 in Test 3), filtering kernels are all 3×3. The results of Test 2 show that the spraying state has little effect on the acquisition of vortex shape image. The UAV itself will not affect the formation of vortex edge images. This method works well under daily light intensity. However, the accuracy of the proposed method decreases to a certain extent under the condition of high illumination intensity. It shows that the method in this paper has some limitations under high intensity illumination.

FIGURE 7. Different filtering kernel edges.

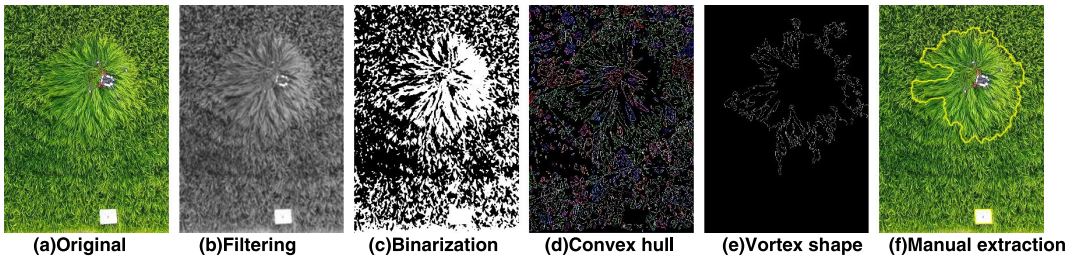

FIGURE 8. Method for Vortex shape retrieval and area calculation based on convex hull algorithm.

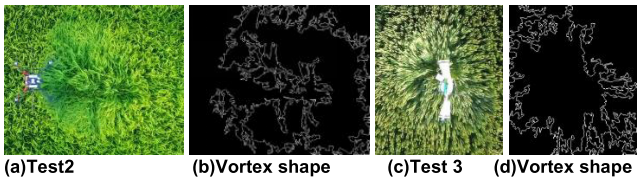

FIGURE 9. Different experimental results.

E. COMPARATIVE ANALYSIS AND ACCURACY VERIFICATION OF THE VORTEX AREA EXTRACTION

The manual extraction method is adopted as the standard for vortex area calculation because the field arrangement of sensors and other equipment will affect the formation of vortex, which has certain follow-up property and cannot be fixed for measurement. The vortex area was extracted manually by comparing the continuous gradient images to determine the actual changed parts, as shown in Fig.7f. According to Equation 5, the total number of pixels of the vortex shape image and the horizontal reference plate extracted by this method is 57068 and 1785, while the number of pixels extracted by manual method is 60123 and 1872, as shown in Fig.7e-f. Thus, the vortex area calculated by the method in this paper is 10.3586m^2, and that calculated by the manual method is 10.4059m^2.

Valid vortex images of Test 1 were extracted from the video shot by the vortex image acquisition system. A total of 650 continuous variation of vortex images were obtained by segmenting them frame. These photos were divided into 50 groups with 13 photos in each group. One of them was randomly selected as the data of this group to calculate the vortex area, as shown in Fig.10.

Based on the vortex area data extracted, according to Equation 6-8, the average error, root mean square error and correlation coefficient were calculated respectively and shown in Tab.3. Comparing results obtained by manual extraction and the method proposed in this paper contributes to the following

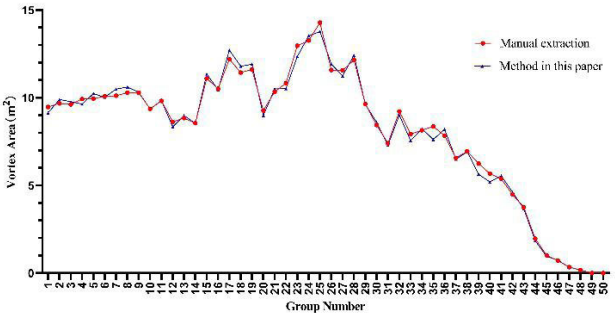

FIGURE 10. Comparison of eddy area calculation results in Test 1.

TABLE 3. Comparative analysis of experimental results

Project	Contrast calculation	
	Method in this paper	Manual extraction
Average error	2.84%	
RMSE	0.2903	
Correlation Coefficient	0.9965	

three findings. First, the average error (p) of 2.84% indicated that error between the two sets of data is small and of high reliability. Second, the root mean square error (RMSE) [26] of 0.2903 implied that the error between the results of this method and the manual extraction is small. Third, the correlation coefficient (r) [27] of 0.9965 suggested that the two sets of data are highly correlated. Compared with the method in this paper, manual method can extract relatively accurate vortex data but it's complicated and inefficient due to the absence of an adaptive mechanism, making it inappropriate to the real-time follow-up study of the vortex. In other words, the proposed method retrieved the edge based on the three characteristics of the vortex image and obtained the vortex

image that reflected the actual state of the vortex in a more satisfactory manner. The method in this paper can effectively replace the manual extraction method.

IV. CONCLUSION

1) According to the method in this paper, the corresponding adaptive binarization iteration threshold can be obtained for vortex images in different environments, and the image preprocessing can be completed by combining with the filtering kernel. Then, the convex hull algorithm combined with edge function can accurately draw the shape of the vortex image. The vortex convex image obtained on the basis of convex hull algorithm reflected the vortex body and details of other parts inside the image which were used to outline the vortex edge.
2) The method proposed in this article was verified by taking 50 groups of vortex images in Test 1 with different vortex shapes and areas as the experimental objects against the reference, namely the manually extracted contour image. The results showed that compared with the manual extraction method, the proposed method reported the average error of 2.84%, the root mean square error of 0.2903, and the correlation coefficient of 0.9965, which indicates that the vortex area calculated by the method described in this paper is closer to the actual value and more reliable. Therefore, it is concluded that the proposed method can replace manual extraction as the standard method for vortex parameter research.
3) The method described in this paper uses the convex hull algorithm to retrieve the accurate vortex image edges, detect the vortex shape and extract its area, filling the gap in adaptive vortex shape retrieval and area extraction. This paper also lays a scientific foundation for the further study of the fine adaptive extraction mechanism of vortex information and real-time follow-up research on UAVs.

The experimental results show that this method is suitable for most of the vortex images, but the precision of the vortex images is reduced under the condition of high intensity illumination. For this problem, it is necessary to design according to the illumination intensity in specific field experiments to balance the influence of illumination intensity. However, in addition to balancing the influence of light, it will also affect the extraction of vortex edges, resulting in the edge points being balanced and unable to be detected. Because field light is average, is not the common one - sided light source. It is worth further study.

It can be observed from the vortex image acquisition platform that the area change of the vortex means that the canopy of the vortex that the UAV gradually rises to the crop during the circling process disappears. This indicates that in a stable environment, the vortex area changes closely related parameters, such as the flight height and speed of the UAV. The method in this paper can accurately extract the vortex image during the motion process, which provides a certain basis and idea for the further study of UAV flight parameters and the real-time variation of vortex. It provides the evidence of calculation data for studying the effects of different scenarios.

REFERENCES

[1] S. Wang, E. Peng, G. Wu, T. Zhang, J. Zhang, C. Zhang, and Y. Yu, "Surveys of deposition and distribution pattern of pesticide droplets on crop leaves," *J. Yunnan Agricult. Univ.*, vol. 25, no. 1, pp. 113–117, 2010, doi: 10.16211/j.issn.1004-390x(n).2010.01.005.

[2] J. Y. Li, S. Guo, W. X. Yao, Y. L. Zhan, and Y. F. Li, "Distribution characteristics of droplet size in rice field and wind tunnel simulation test under airflow operation," *Trans. Chin. Soc. Agricult. Machinery*, vol. 50, no. 8, pp. 148–156, 2019, doi: 10.6041/j.issn.1000-1298.2019.08.017.

[3] L. Jiyu, Y. Lan, W. Jianwei, C. Shengde, H. Cong, L. Qi, and L. Qiuping, "Distribution law of rice pollen in the wind field of small UAV," *Agricult. Sci. Eng. China*, vol. 30, no. 2, pp. 13–19 and 36, 2018, doi: 10.19518/j.cnki.cn11-2531/s.2018.0029.

[4] X. Ping, "Foreground and background segmentation based on superpiexel-level feature representation," *J. Xi'an Univ. Sci. Technol.*, vol. 37, no. 5, pp. 731–735, 2017, doi: 10.13800/j.cnki.xakjdxxb.2017.0520.

[5] J. Liao, D. Jiang, B. Li, Y. Ruan, and Q. Chen, "A nonparametric approach to foreground detection in dynamic backgrounds," *China Commun.*, vol. 12, no. 2, pp. 32–39, Feb. 2015, doi: 10.1109/CC.2015.7084400.

[6] Y. Li, "Fractal dimension estimation for color texture images," *J. Math. Imag. Vis.*, vol. 62, no. 1, pp. 37–53, Oct. 2019, doi: 10.1007/s10851-019-00912-0.

[7] L. Cao, R. Ji, Y. Gao, Y. Yang, and Q. Tian, "Weakly supervised sparse coding with geometric consistency pooling," in *Proc. IEEE Conf. Comput. Vis. Pattern Recognit.*, Jun. 2012, pp. 3578–3585, doi: 10.1109/CVPR.2012.6248102.

[8] J. Hosang, R. Benenson, P. Dollár, and B. Schiele, "What makes for effective detection proposals?" *IEEE Trans. Pattern Anal. Mach. Intell.*, vol. 38, no. 4, pp. 814–830, Apr. 2016, doi: 10.1109/TPAMI.2015.2465908.

[9] D. Yahan, Y. Li, P. Li, and Y. Lyu, "Tree crown outline points extracting and volume calculation based on improved convex hull algorithm," *Eng. Surveying Mapping*, vol. 27, no. 8, pp. 66–71, 2018, doi: 10.19349/j.cnki.issn1006-7949.2018.08.012.

[10] Y. Duan, Q. Wang, X. Li, and Y. Tang, "High-throughput online detection method of egg size and shape based on convex hull algorithm," *Trans. Chin. Soc. Agricult. Eng.*, vol. 32, no. 15, pp. 282–288, 2016, doi: 10.11975/j.issn.1002-6819.2016.15.039.

[11] R. Cupec, I. Vidović, D. Filko, and P. Đurović, "Object recognition based on convex hull alignment," *Pattern Recognit.*, vol. 102, Jun. 2020, Art. no. 107199, doi: 10.1016/j.patcog.2020.107199.

[12] X. Lin, Z.-J. Wang, X. Tan, M.-E. Fang, N. N. Xiong, and L. Ma, "MCCH: A novel convex hull prior based solution for saliency detection," *Inf. Sci.*, vol. 485, pp. 521–539, Jun. 2019, doi: 10.1016/j.ins.2019.02.002.

[13] Y. Wang, Y. Duan, and X. Yuan, "Active contour model based on local enhancement and region fitting," *Appl. Res. Comput.*, vol. 37, no. 8, pp. 1–6, Jul. 2019, doi: 10.19734/j.issn.1001-3695.2019.03.0091.

[14] Y. Bo, S. Luo, and Q. Zhou, "A computational model of salient edges detection on object contour in natural images," *Pattern Recognit. Artif. Intell.*, vol. 23, no. 6, pp. 752–758, 2010, doi: 10.3969/j.issn.1003-6059.2010.06.002.

[15] H. Xie and R. Tong, "Patch-based variational image approximation," *Sci. China Inf. Sci.*, vol. 60, no. 3, pp. 78–87, Mar. 2017, doi: 10.1007/s11432-016-0130-4.

[16] M. A. El Aziz, A. A. Ewees, and A. E. Hassanien, "Whale optimization algorithm and moth-flame optimization for multilevel thresholding image segmentation," *Expert Syst. Appl.*, vol. 83, pp. 242–256, Oct. 2017, doi: 10.1016/j.eswa.2017.04.023.

[17] C. Gao and Y. Zhang, "Fingertip recognition based on a convex hull algorithm," *J. Beijing Univ. Chem. Technol., Natural Sci. Ed.*, vol. 44, no. 2, pp. 70–75, 2017, doi: 10.13543/j.bhxbzr.2017.02.011.

[18] C. Carson, S. Belongie, H. Greenspan, and J. Malik, "Blobworld: Image segmentation using expectation-maximization and its application to image querying," *IEEE Trans. Pattern Anal. Mach. Intell.*, vol. 24, no. 8, pp. 1026–1038, Aug. 2002, doi: 10.1109/TPAMI.2002.1023800.

[19] N. Paramanandham and K. Rajendiran, "Multi sensor image fusion for surveillance applications using hybrid image fusion algorithm," *Multimedia Tools Appl.*, vol. 77, no. 10, pp. 12405–12436, 2017, doi: 10.1007/s11042-017-4895-3.

[20] O. Vincent and O. Folorunso, "A descriptive algorithm for Sobel image edge detection," in *Proc. Informing Sci. + IT Educ. Conf. (SITE)*, 2009, pp. 97–107, doi: 10.28945/3351.

[21] J. Wang, G. Wu, J. Li, and S. K. Jha, "A new method estimating linear Gaussian filter kernel by image PRNU noise," *J. Inf. Secur. Appl.*, vol. 44, pp. 1–11, Feb. 2019, doi: 10.1016/j.jisa.2018.11.002.

[22] J. Canny, "A computational approach to edge detection," *IEEE Trans. Pattern Anal. Mach. Intell.*, vol. PAMI-8, no. 6, pp. 679–698, Nov. 1986, doi: 10.1109/TPAMI.1986.4767851.

[23] X. Chen, W. Yang, and X. Zhu, "Successful treatment of childhood philadelphia chromosome-positive acute myeloid leukemia: Successful treatment for Ph+ AML," *Pediatrics Int.*, vol. 53, no. 4, pp. 598–600, Aug. 2011, doi: 10.1111/j.1442-200X.2010.03262.x.

[24] C.-S. Lee and Y.-H. Kuo, "The important properties and applications of the adaptive weighted fuzzy mean filter," *Int. J. Intell. Syst.*, vol. 14, no. 3, pp. 253–274, 1999, doi: 10.1002/(SICI)1098-111X(199903)14:3<253::AID-INT2>3.0.CO;2-1.

[25] W. Ma, J. Duan, W. Man, H. Zhao, and B. Chen, "Robust kernel adaptive filters based on mean p-power error for noisy chaotic time series prediction," *Eng. Appl. Artif. Intell.*, vol. 58, pp. 101–110, Feb. 2017, doi: 10.1016/j.engappai.2016.11.010.

[26] C. Willmott and K. Matsuura, "Advantages of the mean absolute error (MAE) over the root mean square error (RMSE) in assessing average model performance," *Climate Res.*, vol. 30, no. 1, pp. 79–82, 2005, doi: 10.3354/cr030079.

[27] G. Shan, H. Zhang, and T. Jiang, "Correlation coefficients for a study with repeated measures," *Comput. Math. Methods Med.*, vol. 2020, pp. 1–11, Mar. 2020, doi: 10.1155/2020/7398324.